Chemical Engineering Journal 473 (2023) 145363

Contents lists available at ScienceDirect

Chemical Engineering Journal

journal homepage: www.elsevier.com/locate/cej

Energy storage properties of samarium-doped bismuth sodium titanate-based lead-free ceramics

Xuyao Tang [a], Zimeng Hu [a], Vladimir Koval [b,*], Bin Yang [c], Graham C. Smith [c], Haixue Yan [a,*]

[a] School of Engineering and Materials Science, Queen Mary University of London, Mile End Road, London E1 4NS, UK
[b] Institute of Materials Research, Slovak Academy of Sciences, 04001 Kosice, Slovakia
[c] Faculty of Science & Engineering, University of Chester, Parkgate Road, Chester CH1 4BJ, UK

ARTICLE INFO

Keywords:
Energy storage capacitors
Lead-free
Relaxor ferroelectrics
Ceramics
Samarium

ABSTRACT

Due to worldwide environmental regulations, lead-free relaxors, namely $Bi_{0.5}Na_{0.5}TiO_3$–$6BaTiO_3$ (BNT-6BT) are being extensively studied as an alternative candidate for energy storage applications. Here, Sm was introduced at different A sites of the relaxor system; specifically, the Sm-doped BNT-6BT system was designed to replace Bi (BNT-Bi), Na (BNT-Na), and both the Bi and Na ions (BNT-BiNa) by Sm ions. It was found that the BNT-Bi sample possesses high piezoelectricity (d_{33} = 117.3 pC N^{-1}), whereas the BNT-Na and BNT-BiNa ceramics show exceptionally high values of the energy storage density and efficiency. To define the energy storage performance, a new concept based on determining the recoverable energy storage intensity is proposed in the present work. This allows bypassing the high applied electric fields in determining the value of the energy storage density. An ultrahigh recoverable energy storage density (4.41 J cm^{-3}), excellent energy storage efficiency (83.96%) and superhigh recoverable energy storage intensity (19.17 × 10^{-3} J kV^{-1} cm^{-2}) were achieved in the BNT-BiNa ceramics simultaneously. Furthermore, the energy storage characteristics exhibit an excellent stability over a wide temperature range from 25 °C to 150 °C. Thus, the developed Sm-doped BNT-6BT ceramics show great potential for piezoelectric and high-power energy storage applications.

1. Introduction

The growing world population brings about a huge increase in energy consumption. In 2019, more than three-quarters of the world's energy resources were from fossil fuels, [1] the conversion of which to energy can emit large amounts of greenhouse gases. Therefore, there is not only the problem of fossil fuel depletion, but also environmental pollution and global warming. [2] The development of various clean and renewable energy sources is an obvious and feasible solution. [2–5] Nuclear, hydro, geothermal, solar and wind energy generation technologies are becoming important resources to replace the fossil fuel energy systems. [5] However, these renewable energy sources are intermittent and difficult to use continuously. [3,5] Reliable and efficient electrical energy storage solutions are key to the efficient generation of electrical energy from renewable sources.

Due to their high-power energy storage density, low-cost production and excellent energy storage stability, dielectric capacitors (electrostatic capacitors) are widely used in high power energy storage applications. [6–8] An extensive number of studies have reported on high energy density in ferroelectric thin films. [9,10] The use of bulk ceramics in energy storage industry has, however, many advantages over the films mainly owing to their low cost and high effective volume for storing energy. In recent years, lead-free ceramics have attracted increasing attention due to the health concern related to toxicity of lead and environmental protection. [10–16] A solid solution of bismuth sodium titanate and barium titanate, (1-x)$Bi_{0.5}Na_{0.5}TiO_3$-x$BaTiO_3$ (abbreviated as BNT-xBT) was initially studied by Takenaka *et al.* in 1991. [17] It was shown that the perovskite system exhibits good piezoelectric and ferroelectric properties near the morphotropic phase boundary (MPB) separating the rhombohedral (R) and tetragonal (T) phases. The MPB composition of the BNT-BT system corresponds to x = 0.06–0.07, where the difference of free energies of the two phases is minimal. Even that the understanding of relaxor-like behaviour of BNT is still under debate, there is a consensus that it undergoes electric field-induced transitions from a relaxor to stable ferroelectric state characterized by a large polarization (over 35 μC cm^{-2}). [17,18] The high value of the remanent polarization and relaxor features (e.g., slim ferroelectric hysteresis loop) make BNT a promising material for efficient storage of electrical energy.

* Corresponding authors.
E-mail addresses: vkoval@saske.sk (V. Koval), h.x.yan@qmul.ac.uk (H. Yan).

https://doi.org/10.1016/j.cej.2023.145363
Received 20 April 2023; Received in revised form 29 June 2023; Accepted 9 August 2023
Available online 11 August 2023

A partial substitution of lead-based ferroelectrics with samarium (Sm) has been demonstrated to improve their piezoelectric properties. [19–21] On the other hand, the Sm substitution at certain concentrations was found to reduce the thermal stability of piezoelectric constants of lead-based materials. [19,22] These findings motivated us to study the effect of Sm, occupying different A-site positions in the BNT perovskite, on the piezoelectric and energy storage properties of the lead-free BNT-BT relaxor ceramics.

In the present work, lead-free $0.94Bi_{0.5}Na_{0.5}TiO_3$-$0.06BaTiO_3$ (abbreviated as BNT-6BT) ceramics doped by 2.5 mol% of Sm was prepared by the conventional ceramic route and characterized for the piezoelectric and energy storage properties. The Sm substitution includes the replacement of Bi, Na and both the Bi and Na ions in the BNT lattice. Accordingly, the first composition is $0.94Bi_{0.4734}Sm_{0.0266}Na_{0.5}TiO_3$ $-0.06BaTiO_3$ (abbreviated as BNT-Bi), the second composition is $0.94Bi_{0.5}Na_{0.4202}Sm_{0.0266}TiO_3$ $-0.06BaTiO_3$ (abbreviated as BNT-Na), and the third composition is $0.94Bi_{0.4867}Sm_{0.0133}Na_{0.4601}Sm_{0.0133}TiO_3$ $-0.06BaTiO_3$ (abbreviated as BNT-BiNa). By a comprehensive structural and electrical property analysis, it is demonstrated that the localisation of the Sm ions at the different A sites largely affects the functional properties of the BNT-6BT ceramics. While the BNT-Bi sample shows a high piezoelectric d_{33} coefficient, other two compositions are nearly non-piezoelectric. On the other hand, the BNT-Na and BNT-BiNa ceramics exhibit excellent dielectric and energy storage properties. Particularly, the latter with the ultrahigh recoverable energy storage density (4.41 J cm^{-3}), excellent energy storage efficiency (83.96%) and superior recoverable energy storage intensity (19.17 $\times$ 10^{-3} J kV^{-1} cm^{-2}) is a promising candidate for high-power energy storage applications. The improved energy storage properties (incl. thermal stability of the storage performance) of the ceramic where Sm ions replace randomly both Bi and Na ions at the A sites are related to the enhanced relaxor behaviour.

2. Material and methods

The ceramic samples of BNT-Bi ($0.94Bi_{0.4734}Sm_{0.0266}Na_{0.5}TiO_3$ $-0.06BaTiO_3$), BNT-Na ($0.94Bi_{0.5}Na_{0.4202}Sm_{0.0266}TiO_3$ $-0.06BaTiO_3$) and BNT-BiNa ($0.94Bi_{0.4867}Sm_{0.0133}Na_{0.4601}Sm_{0.0133}TiO_3$ $-0.06BaTiO_3$) were prepared by the conventional solid-state reaction method. The starting materials were Sm_2O_3 (purity $\geq$ 99.9%, Alfa Aesar), Bi_2O_3 ($\geq$99.9%, Aldrich), Na_2CO_3 ($\geq$99.5%, Sigma-Aldrich), TiO_2 ($\geq$99.8%, Sigma-Aldrich), $BaCO_3$ ($\geq$99.8%, Alfa Aesar). The raw powders were dried at 200 °C for 20 h before being weighted. After weighting according to the stoichiometric formulae, they were thoroughly mixed and milled for 5 h in ethanol using a planetary mill (Pulverisette 5, Fritsch) and zirconia balls. The mixture was dried overnight in air. Then, the mixture was calcined at 800 °C for 2 h, followed by the second-level calcination at 900 °C for 4 h. To reduce the size of the particles, a milling of the calcined precursors was carried out for 4 h in ethanol using the planetary mill. During the last 10 min of milling, a binder (5 wt% polyvinyl alcohol solution) was added to the powder for a better compaction of the samples. After drying the mixture of the calcined powder and binder, it was cold pressed into pellets (a diameter of 13 mm and thickness of 1 mm) under 200 MPa. The pellets were annealed at 800 °C for 2 h in order to remove the polyvinyl alcohol binder. Sintering of the ceramics was carried out for 4 h at a temperature between 1100 °C and 1120 °C, depending on the chemical composition.

The relative density of all the sintered samples was found to be above 96%, as determined by the Archimedes' method. The crystal structure of the sintered samples at room temperature was identified on the crushed ceramic powders by X-ray diffraction (XRD, PANalytical X'Pert Pro X-ray diffractometer, PANalytical, Cambridge, UK) utilizing Cu-Kα radiation. Scanning electron microscopy (SEM, a FEI Inspect F microscope, Hillsboro, OR, USA) was used to observe microstructures of the sintered ceramics. An Energy Dispersive X-ray (EDX) spectrometer (Oxford Instruments, UK) attached to the SEM microscope was employed to perform an elemental mapping of the samples. Raman spectroscopy of the polished ceramic samples was performed with a LabRam microprobe system (ISA/Jobin-Yvon/Horiba, France). An Ar ion laser with 638 nm wavelength was used for excitation, and a 100x microscope objective lens was employed to focus and collect the scattered light. The Raman scattering data were collected with a Peltier-cooled charged coupled device camera from 100 to 950 cm^{-1} with a step of 0.5 cm^{-1} and an integration time of 10 s, while keeping the laser power below 3 mW to prevent a local overheating. X-ray Photoelectron Spectroscopy (XPS) spectra were acquired using a monochromated AlKα X-ray source (a model Focus 500, Specs GmbH, Germany) and hemispherical analyser (a model PHOIBOS 150, Specs GmbH, Germany). The XPS spectra (high-resolution scans) were obtained using a pass energy of 20 eV. The energy scale of the XPS unit was calibrated according to the ISO standard 15472 (the C 1 s spectrum at 285.0 eV). The XPS data were fitted by using a CasaXPS software v2.3.16 (Casa Software Ltd, Teignmouth, UK).

Ag electrodes were fabricated by using a silver paste (Gwent Electronic Materials Ltd., C2011004D5, Pontypool, UK). They cover major surfaces of the disks with a diameter of 10 mm and thickness of about 1 mm. The dielectric permittivity and loss tangent of the prepared samples at various frequencies from 100 Hz to 10 MHz were measured by a precision impedance analyser (a model 4294A, Agilent, Hyogo, Japan). All samples were poled at room temperature in a direct current (DC) field of 50 kV cm^{-1} for 10 min with a high voltage power supply (a model 2807, Alpha Series II, Brandenburg, Germany). The piezoelectric coefficient (d_{33}) of the poled samples was measured by a quasi-static d_{33} meter (a model ZJ-3B, Chinese Academy of Sciences, China). The temperature dependence of the dielectric permittivity and loss tangent at various frequencies in the range of 100 Hz – 1 MHz was measured using an LCR meter (a model 4284A, Agilent, Hyogo, Japan) attached to a PC controlled furnace. A ferroelectric tester (NPL, Teddington, U.K.) was used to acquire the current-electrical field (*I-E*) and polarization-electrical field (*P-E*) hysteresis loops of the samples immersed in a silicone oil bath. The ferroelectric hysteresis loops were collected over a wide temperature range from 25 °C to 150 °C at a frequency of 10 Hz. For the ferroelectric property measurements, the BNT-Na and BNT-BiNa samples were polished to a thickness of 0.11–0.14 mm, and then coated by gold. The Au electrodes with a diameter of 2 mm were deposited on the major opposite surfaces of samples. The values of the energy storage density and energy storage efficiency were obtained from the *P-E* hysteresis loop, as collected at various temperatures and maximum applied switching electric fields.

3. Results and discussion

Using the conventional ceramic route, dense and highly uniform (chemically and structurally) ceramics of BNT-Bi, BNT-Na and BNT-BiNa with tightly bounded grains were prepared (in Supporting Information, Fig. S1 shows SEM images of a fracture surface of the samples; Fig. S2, Fig. S3, and Fig. S4 show EDX mapping and semi-quantitative analysis of the selected chemical elements in the respective samples of BNT-Bi, BNT-Na, and BNT-BiNa). In BNT-Bi, where Sm partially replaces Bi, the EDX analysis shows a slightly lower content of Bi compared to Na. Similarly, in BNT-Na, where Sm partially replaces Na, a slightly lower content of Na compared to Bi was found by EDX spectroscopy. In BNT-BiNa, where Sm simultaneously replaces both Bi and Na, the EDX analysis indicates that the contents of Bi and Na are almost identical. These findings suggest that Sm enters the required positions in the designed ceramic systems.

The Rietveld method fitted XRD patterns of the BNT-Bi, BNT-Na and BNT-BiNa ceramics are shown in Fig. 1.

From the figure, it is clear that BNT-Bi has a perovskite structure without any traces of a secondary phase (within the detection limit of the diffractometer). This observation suggests that Sm enters the BNT-BT lattice, occupying the A sites of the perovskite. The Rietveld analysis of the XRD data revealed that BNT-Bi is a bi-phasic material,

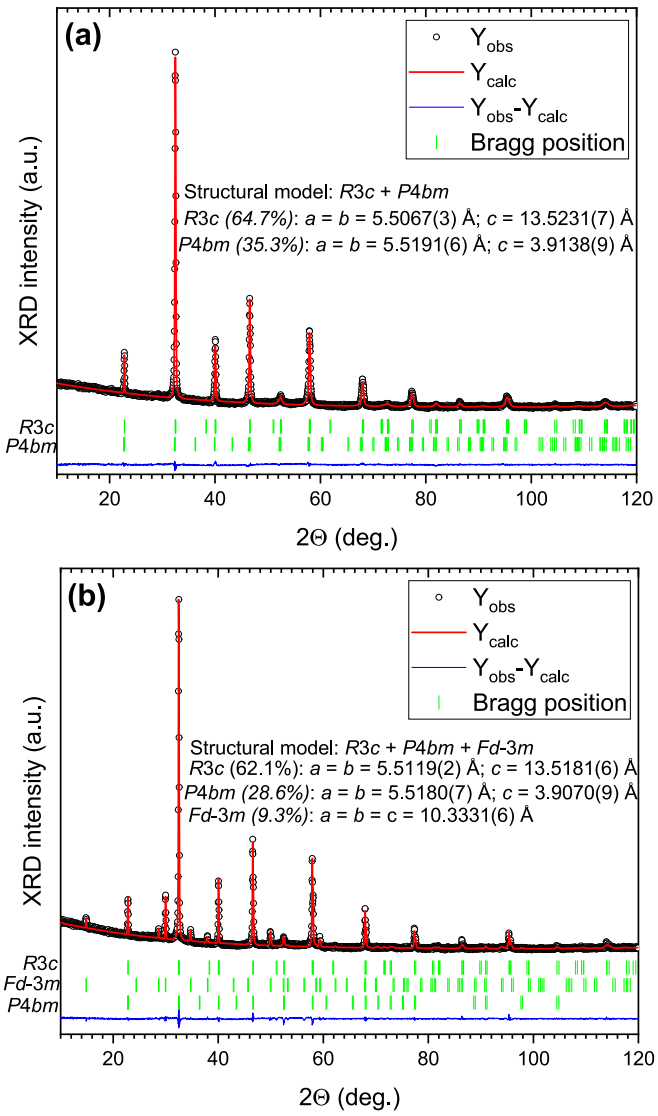

Fig. 1. The fitted XRD patterns of (a) BNT-Bi, (b) BNT-Na, and (c) BNT-BiNa.

consisting of a rhombohedral (a space group, SG: *R3c*) phase and a tetragonal (SG: *P4bm*) phase. The rhombohedral *R3c* phase is polar and prevails (a phase fraction: 64.7%) in the material. The refined lattice constants of the *R3c* structure are: $a = b = 5.5067$ Å, and $c = 13.5231$ Å. The lattice parameters of the weakly polar *P4bm* phase were estimated to be: $a = b = 5.5191$ Å, and $c = 3.9138$ Å.

Unlike the bi-phasic BNT-Bi sample, the crystal structure of BNT-Na contains, in addition to the *R3c* and *P4bm* phases, a secondary phase with a cubic symmetry (SG: *Fd*-3 *m*). This impurity is of a pyrochlore type $Sm_2Ti_2O_7$ with the lattice constant of about 10.3331 Å. It contributes to the XRD pattern by 9.3%, but does not affect ferroelectric properties of the material because cubic pyrochlores are not polar materials. The estimated contribution and the lattice parameters of the *R3c* phase and the weak polar *P4bm* phase are shown in Table 1.

BNT-BiNa adopts at room temperature, similarly to BNT-Bi, the two-phase perovskite structure, where the amount of the polar *R3c* phase is about 59%. The lattice constants of the *R3c* and *P4bm* phases are given in Table 1. The *c*-constant is decreased in both phases, if compared to these in BNT-Bi, while as the refined lattice parameters *a* and *b* are increased in the *R3c* phase. The substitution of larger ions of Bi^{3+} (ionic radius ~ 1.40 Å, coordination number CN = 12) and Na^{+} (ionic radius ~ 1.39 Å, CN = 12) ions with smaller Sm^{3+} ions (ionic radius ~ 1.24 Å, CN = 12) results in the observed change of the lattice parameters. [23].

According to the results of XRD refinements, the composition of all three ceramic samples belongs to the MPB region of the BNT-6BT system. The MPB composition of the samples was also evidenced by Raman spectroscopy. [18,24] The Raman spectra from 100 to 950 cm^{-1} were successfully deconvoluted and assigned to two perovskite-structured phases - rhombohedral phase (a characteristic Raman active mode ~ 253 cm^{-1}) and tetragonal phase (a characteristic Raman active mode ~ 312.5 cm^{-1}) (Fig. S5 in Supporting Information).[24].

Fig. 2 shows the dielectric permittivity and loss tangent as a function of frequency (from 100 Hz to 10 MHz) for the unpoled and poled BNT-Bi, BNT-Na, and BNT-BiNa ceramics at room temperature. As can be seen, the relative dielectric permittivity decreases and loss tangent increases with increasing frequency. Such behavior can be attributed to the dielectric relaxation which is related to different polarization mechanisms having different relaxation times. At low frequency, polarizations with different relaxation time can be active and contribute to the dielectric permittivity. When the frequency is increased, the slow polarization processes are not able to keep up with the applied electric alternating current (AC) field, leading to the decrease in the permittivity and increase of the dielectric loss [25–27].

From Fig. 2(a), one can see that after poling at a DC field of 50 kV

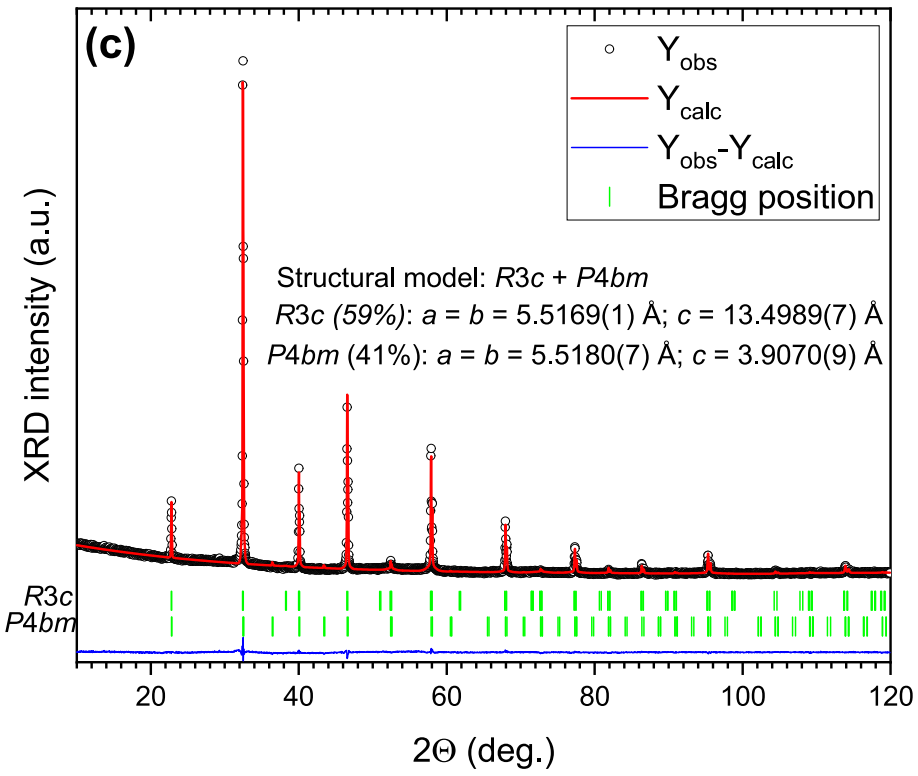

Fig. 1. (*continued*).

Table 1
Crystal structure refinement parameters of BNT-Bi, BNT-Na and BNT-BiNa.

Sample	Unit cell parameters (Å) (Phase 1, *R*3*c*)	Unit cell parameters (Å) (Phase 2, *P4bm*)	Unit cell parameters (Å) (Phase 3, *Fd*-3 *m*)	Weight fraction (%)	*R*-factors and GOFs
BNT-Bi	$a = b =$ 5.5067(3) $c =$ 13.5231 (7) $\alpha = \beta = 90°$, $\gamma = 120°$ Volume = 355.53(4) (Å^3)	$a = b =$ 5.5191(6) $c =$ 3.9138 (9) $\alpha = \beta = \gamma =$ 90° Volume = 119.22(6) (Å^3)		*R3c* = 64.7 *P4bm* = 35.3	*Rp* = 20.7 *Rwp* = 12.4 *Rexp* = 7.62 χ^2 = 2.07
BNT-Na	$a = b =$ 5.5119(2) $c =$ 13.5181 (6) $\alpha = \beta = 90°$, $\gamma = 120°$ Volume = 355.20(2) (Å^3)	$a = b =$ 5.5180(7) $c =$ 3.9070 (9) $\alpha = \beta = \gamma =$ 90° Volume = 118.96(2) (Å^3)	$a = b = c =$ 10.3331(6) $\alpha = \beta = \gamma =$ 90° Volume = 1101.35(7) (Å^3)	*R3c* = 62.1 *P4bm* = 28.6 *Fd*-3 *m* = 9.3	*Rp* = 31.0 *Rwp* = 18.2 *Rexp* = 8.7 χ^2 = 3.64
BNT-BiNa	$a = b =$ 5.5169(1) $c =$ 13.4989 (7) $\alpha = \beta = 90°$, $\gamma = 120°$ Volume = 355.65(6) (Å^3)	$a = b =$ 5.5180(7) $c =$ 3.9070 (9) $\alpha = \beta = \gamma =$ 90° Volume = 118.96(2) (Å^3)		*R3c* = 59.0 *P4bm* = 41.0	*Rp* = 27.4 *Rwp* = 14.2 *Rexp* = 7.65 χ^2 = 2.71

Note: GOF (χ^2) represents the goodness of fit.

cm^{-1}, the dielectric permittivity (ε_r) of the BNT-Bi ceramic is decreased and the dielectric losses (tanδ) are increased in the entire range of frequencies used. The decrease of dielectric permittivity after poling indicates that some contribution to the permittivity is extrinsic, originating from switchable domain walls. Ferroelectric domains become larger during DC poling and at the same time the number of the domain walls is reduced, that means the decrease in the domain wall density. As a consequence, the dielectric permittivity of the sample is decreased on poling. The increase of the dielectric loss after poling is believed to be caused also by the larger domains. [28] In addition, a series of permittivity peaks reflecting the piezoelectric activity of the sample (the 1st and 2nd harmonic resonances) can be observed in the dielectric spectra (ε_r and tanδ *vs.* frequency). The poled BNT-Bi sample exhibits a high piezoelectric d_{33} coefficient (~117.3 pC N^{-1}), which is comparable to the value reported earlier for BNT-6BT ceramics (Fig. S6 in Supporting Information). [17,29–32] It is worth mentioning that the poling at 50 °C resulted in reduction of d_{33} to 84.1 pC N^{-1}, pointing to the effect of the thermal depolarization. This phenomenon will be further discussed along with the analysis of the temperature dependence of the dielectric properties and ferroelectric polarization behaviour at high temperatures. The value of d_{33} of the poled BNT-Na and BNT-BiNa ceramics is small, close to 3 pC N^{-1}. These two samples, in addition, show no obvious change in the dielectric permittivity on poling, which suggests the reversible field-induced transitions.

Fig. 3 shows the temperature dependence of the dielectric permittivity and loss tangent at five different frequencies (1 kHz, 10 kHz, 100 kHz, 500 kHz and 1 MHz) for the unpoled BNT-Bi, BNT-Na, and BNT-BiNa ceramics (for the poled samples see Figure S7, in Supporting Information). It is generally accepted that the dielectric behaviour of BNT-6BT ceramics shows a strong frequency dispersion. [33] Moreover, when heated from room temperature, the BNT-6BT relaxor system exhibits two distinct anomalies in the dielectric permittivity/ loss against temperature curves. The first anomaly at lower temperatures, i.e., where a shoulder starts to develop, defines the depolarization temperature (T_d). This temperature corresponds to the phase transition temperature

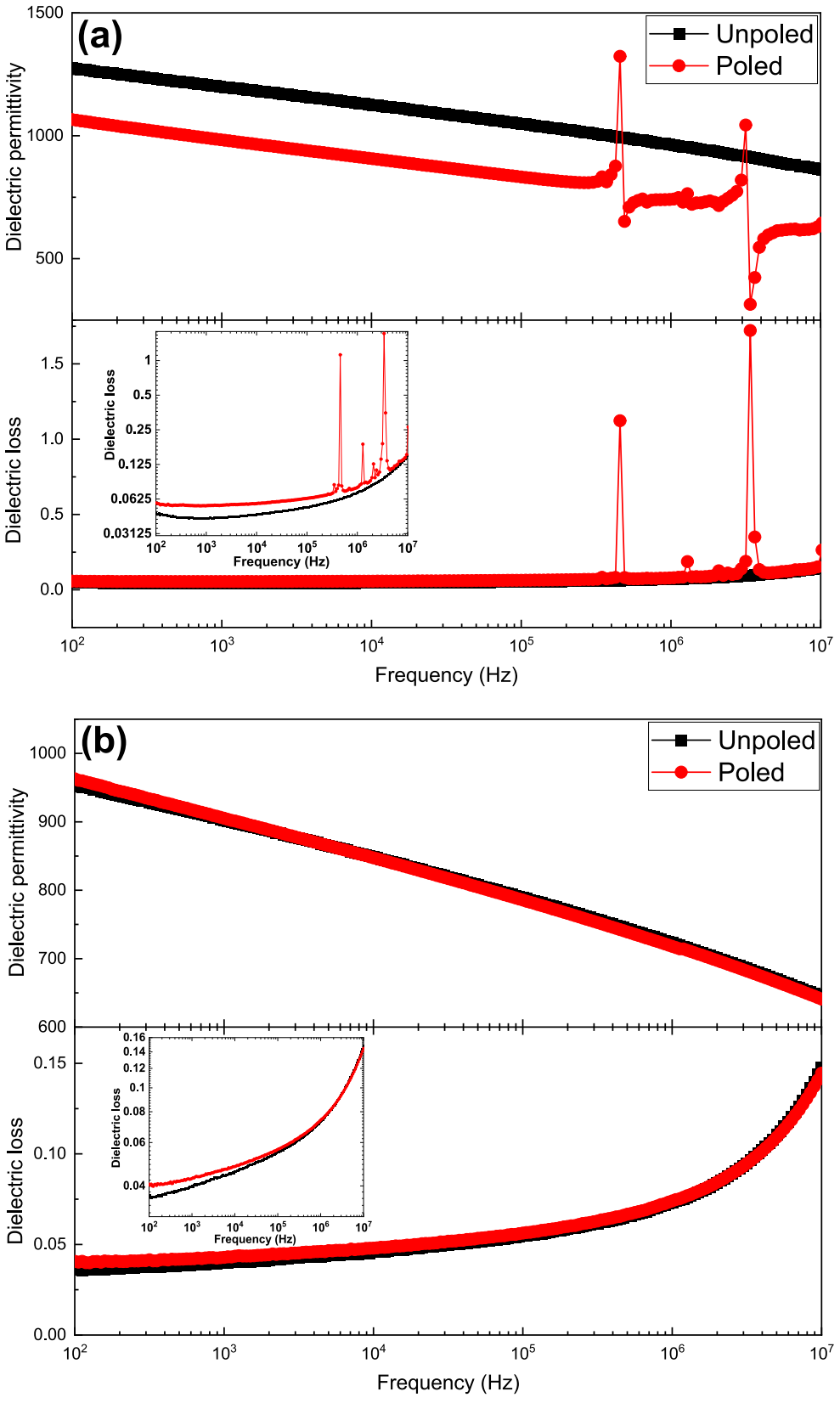

Fig. 2. Frequency dependence of the dielectric permittivity and loss for the unpoled and poled samples at room temperature: (a) BNT-Bi, (b) BNT-Na, and (c) BNT-BiNa (the inset shows the dielectric loss as a function of frequency in log scale).

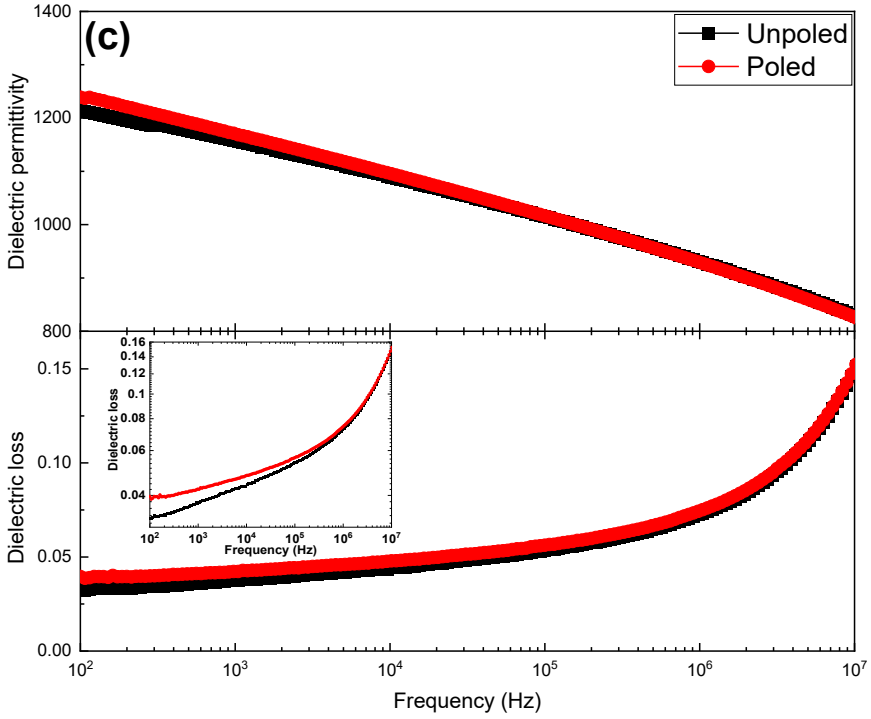

Fig. 2. (*continued*).

from ferroelectric (FE) phase to relaxor phase, and can be identified also as the temperature of the fastest decrease of the remanent polarization. [34,35] Here, T_d is determined from the hump of the dielectric loss versus temperature curves of the unpoled samples (Fig. 3(a)-Fig. 3(c)). [33,36] The second anomaly occurs in the higher temperature region and corresponds to the temperature of the maximum permittivity (T_m). Because of the relaxor behaviour, T_m is not considered a Curie point of the ferroelectric-to-paraelectric transition. [34,37].

For BNT-Bi, the temperatures T_d and T_m of the unpoled sample are about 126 °C and 236 °C, respectively, which are close to the values reported by other researchers for pure BNT-6BT. [31] Also, the values of the dielectric permittivity of BNT-Bi at room temperature and at T_m are in accordance with the earlier studies. [31,33,38] For the poled sample, T_d and T_m are about 85 °C and 236 °C. The depolarization temperature of the poled BNT-Bi sample is lower than that of the unpoled ceramic, which implies a reduced temperature stability of piezoelectricity. It is proposed that the limited piezoelectric stability of the Sm-doped BNT-6BT ceramics, if compared to pure BNT-6BT, [31,33] is a result of the lowering of T_d by the Sm doping. An introduction of Sm ions at Pb sites has also been found to deteriorate the thermal stability of piezoelectric constants of lead-based materials. [19,22].

For the second composition, the T_d and T_m of the unpoled and poled BNT-Na ceramics are nearly same, about 64 °C and 286 °C, respectively. Similarly, the depolarization temperature and maximum permittivity temperature for the unpoled and poled BNT-BiNa samples are almost identical, $T_d \sim 65$ °C and $T_m \sim 289$ °C. A small difference in the values of T_d and T_m of BNT-Bi, BNT-Na and BNT-BiNa can be attributed to temperature measurement error. The dielectric permittivity of these two ceramics is lower than that of pure BNT-6BT. [31,33] In addition, from Figs. 2 and 3, one can infer that the dielectric permittivity of the BNT-Bi sample is the highest, and that the permittivity of BNT-BiNa is higher than of BNT-Na. Higher dielectric permittivity yields the lower breakdown electric field strength of relaxor ferroelectrics. [8] The decreased breakdown field significantly affects the energy storage density of these materials. As shown in Fig. 4(b) and (c), the breakdown electric field strength of the BNT-Na ceramic (260 kV cm^{-1}) is higher than that of the BNT-BiNa ceramic (230 kV cm^{-1}).

The temperatures T_d and T_m of the BNT-Na and BNT-BiNa ceramics change only a little on poling. This can be explained by assuming that BNT-Na and BNT-BiNa relaxors contain a higher number of polar nano regions. These can be reversed by an external electric field upon field removal. Similar behaviour was observed in BNT-BT ceramics with high density of the nano-sized polar regions. [39] It should be mentioned that the BNT-Na and BNT-BiNa ceramics show low dielectric loss (Fig. 3(b) and (c)), which is beneficial for energy storage applications.

In Fig. 3(b) and Fig. 3(c), the permittivity increases and dielectric loss decreases with increasing temperature in the temperature region between T_d and T_m. This behaviour can be attributed to the transformation of thermally stable ferroelectric domains into thermally active polar nano regions (PNRs). Presumably, a high concentration of PNRs is responsible for the increased permittivity. For dielectric loss, there are two contributions - DC conductivity and friction between dipoles. [40] At high temperatures, the contribution of DC conductivity to dielectric loss increases. In Fig. 3(b) and Fig. 3(c), the decrease of loss with increasing temperature indicates that the dielectric loss in the temperature range T_d - T_m is not dominated by the DC conductivity, but frictions between PNRs under applied AC field. These decrease at higher temperatures largely, resulting in the loss reduction.

As shown in Fig. 3, the temperature dependencies of the dielectric permittivity of the Sm-doped samples show a strong frequency dispersion. For BNT-Na and BNT-BiNa, the frequency dispersion is clearly seen in the low temperature region, around T_d (Fig. 3(b) and (c)). Upon further heating, the dispersion gradually disappears. On the other hand, in the BNT-Bi sample, the frequency dependency of the dielectric permittivity exists from room temperature up to 600 °C. Such behaviour is thought to be caused by the thermal activation of mobile charge carriers, such as oxygen vacancies. [41] The crystal structure of BNT-based ceramics typically consists of a strong polar *R3c* phase and a weak polar *P4bm* phase. For the occurrence of the dielectric relaxation and distinct T_d temperature in these ferroelectrics is mainly responsible the tetragonal *P4bm* phase. [38,42] However, the structure of the studied BNT-Bi sample is predominantly composed of the rhombohedral *R3c* phase, which makes difficult to clearly identify T_d in the permittivity *vs.* temperature plot. The strong polar nature of BNT-Bi is also consistent

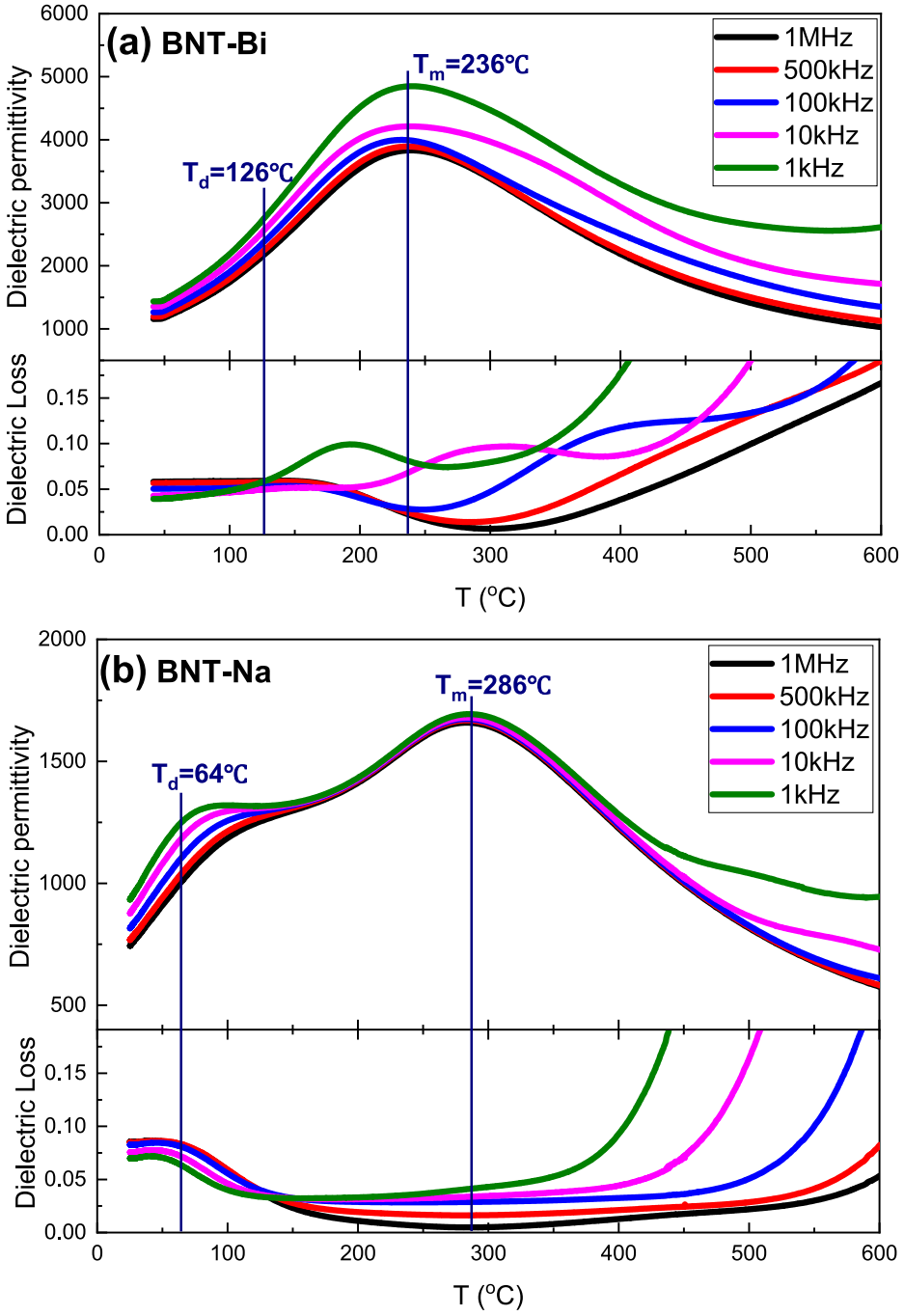

Fig. 3. Temperature dependence of the dielectric permittivity and loss at five different frequencies for the unpoled ceramic samples of (a) BNT-Bi, (b) BNT-Na, and (c) BNT-BiNa.

with the higher distortion ($c/a = 2.456$) of the *R*3*c* phase, if compared to that of BNT-6BT ($c/a = 2.436$). [43].

In order to investigate oxygen vacancies in the prepared samples, X-ray photoelectron spectroscopy (XPS) has been employed. [44,45] Fig. S8 - Fig. S10 (in Supporting Information) display the XPS spectra of O 1s, Ti 2p, Bi 4d, Bi 4f, Ba 3d, Na 1s and Sm 3d for the BNT-Bi, BNT-Na and BNT-BiNa ceramics. As the concentrations of Ba, Na and Sm ions are rather low, the noise level of the scans over the 3d peaks is high. The O 1s spectra of the three ceramics are composed of three spectral peaks located at the binding energy of about 529.8 eV, 531.3 eV and 532.5 eV, which can be ascribed to the lattice oxygen (O 1s I), oxygen vacancies (O 1s II) and chemically absorbed oxygen species (O 1s III). [44,46,47] By analysis of the oxygen XPS spectra, it was found that an amount of oxygen vacancies in all the samples is about 33.77% − 37.58%, which is very close to each other. The temperature dependencies of the dielectric permittivity and loss of BNT-Na and BNT-BiNa are nearly stable, which suggests only a weak influence of the oxygen vacancies. Thus, one can propose that the donor doping in the BNT-Na and BNT-BiNa ceramics (Na^+ substituted by Sm^{3+}) is compensated by the A-site sodium vacancies, which are negatively charged and difficult to move. On the other hand, the positively charged oxygen vacancies are highly mobile at moderate temperatures and under high electric fields. [48] In the BNT-Na and BNT-BiNa ceramics, oxygen vacancies are attracted by the negative sodium vacancies. Therefore, even though the presence of

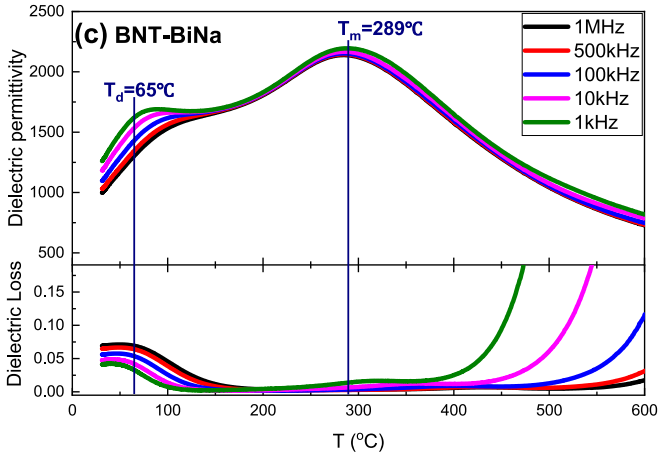

Fig. 3. (*continued*).

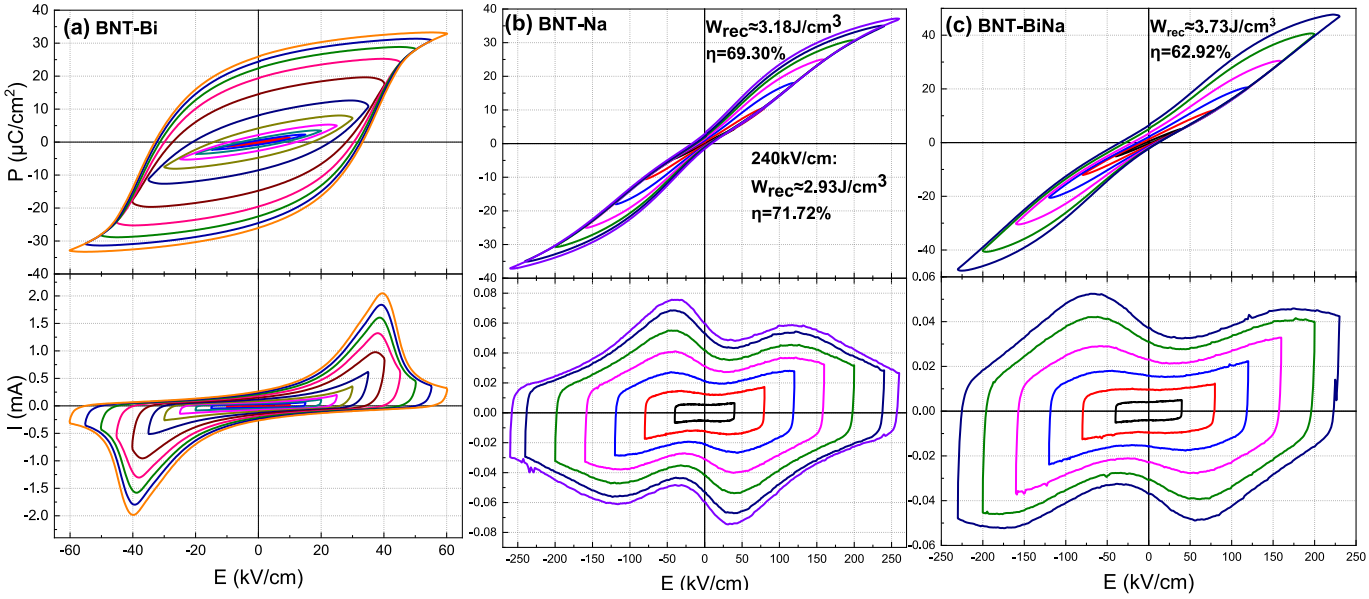

Fig. 4. *P-E* and *I-E* loops of (a) BNT-Bi, (b) BNT-Na, (c) BNT-BiNa ceramics, as obtained at room temperature.

oxygen vacancies in BNT-Na and BNT-BiNa is clearly demonstrated by XPS, they are inactive and do not affect the temperature dependencies of the dielectric permittivity and loss. In the BNT-Bi sample, the oxygen vacancies are electrically active and have a large impact on the dielectric properties.

The polarization–electric field (*P-E*) hysteresis loops and current-electric field (*I-E*) hysteresis loops of the BNT-Bi, BNT-Na, and BNT-BiNa samples under various applied electric fields at room temperature are shown in Fig. 4. The values of the remanent polarization (P_r), as obtained from the *P-E* hysteresis loops, are summarized in Table S1 (in Supporting Information). The *P-E* and *I-E* loops of the BNT-Bi ceramic indicate a conventional ferroelectric behaviour characterized by the large P_r (25.88 μC cm^{-2}) and typical domain switching current peaks. The high remanent polarization, if compared to that of the BNT-Na and BNT-BiNa samples, make the BNT-Bi ceramics a suitable material for piezoelectric applications. [49,50] On the other hand, double *P-E* hysteresis loops with the field-induced increased saturated polarization and low remanent polarization pre-determine the BNT-Na and BNT-BiNa ceramics for energy storage applications.

In BNT-6BT ceramics, Bi^{3+} ions relative to the *R*3*c* cell are responsible for regular ferroelectric (FE) order and occurrence of ferroelectricity. [51] They also play a prominent role in local atomic disorder at A sites of the BNT-6BT relaxor system. [52] In our samples, when Bi^{3+} ions are partly replaced by isovalent ions of samarium, the piezoelectric constant d_{33} of the BNT-Bi ceramic does not change significantly, but the depolarization temperature is lowered, if compared to pure BNT-6BT ceramics. [38] Hence, the Sm doping is beneficial to the enhancement of energy storage performance of BNT-6BT.

The polar phase with the tetragonal *P*4*bm* structure of the BNT-6BT system is predominantly formed by short-range ordered nanodomains of a size of about 100 nm, which give rise to the relaxor behaviour. [33,53] When the Sm^{3+} ion is in place of Na^+, the ferroelectric order is suppressed and the remanent polarization (P_r) is decreased. Consequently, the *P-E* loop of the BNT-Na sample is slim, providing the improved energy storage properties. In addition, samarium, as a member of the rare earth family, can reduce the leakage current and increase the breakdown field strength. [54].

Comparing the *P-E* loops in Fig. 4, it is clear that, at the same maximum switching field, the saturated polarization of the BNT-BiNa ceramic is bigger than that of the BNT-Na. However, it is lower than that of the BNT-Bi sample. Thus, one can propose that the partial substitution of Bi^{3+} ions by Sm^{3+} ions improve the saturated polarization. As the ionic radius of Sm^{3+} is smaller than that of Bi^{3+}, [23] the Sm doping introduces a structural distortion in the BNT lattice and, thus,

affects the ferroelectric polarization. [55] The BNT-BiNa sample exhibits a much lower remanent polarization (6.37 μC cm^{-2}) than BNT-Bi (25.88 μC cm^{-2}), but higher than that displayed by the BNT-Na ceramic (2.87 μC cm^{-2}). Therefore, even the *P-E* loops of BNT-Na are slimmer than these of BNT-BiNa, the high saturated polarization favours the latter for using in energy storages because it may produce a higher storage density.

The energy storage density (W), recoverable energy storage density (W_{rec}) and energy storage efficiency (η) can be calculated from the measured *P-E* hysteresis loop using the following formulae: [56,57]

$$W = \int_0^{P_{max}} EdP \tag{1}$$

$$W_{rec} = \int_{P_r}^{P_{max}} EdP \tag{2}$$

$$\eta = \frac{W_{rec}}{W} \times 100\% \tag{3}$$

where P_{max} is the saturated polarization, P_r is the remanent polarization and E is the applied external electric field. From the above formulae, it can be concluded that the larger breakdown electric field strength, the lower remanent polarization, and the larger saturated polarization would effectively improve W_{rec} and η. In this perspective, relaxor ferroelectrics have greater potential for energy storage applications than normal ferroelectrics and antiferroelectrics.

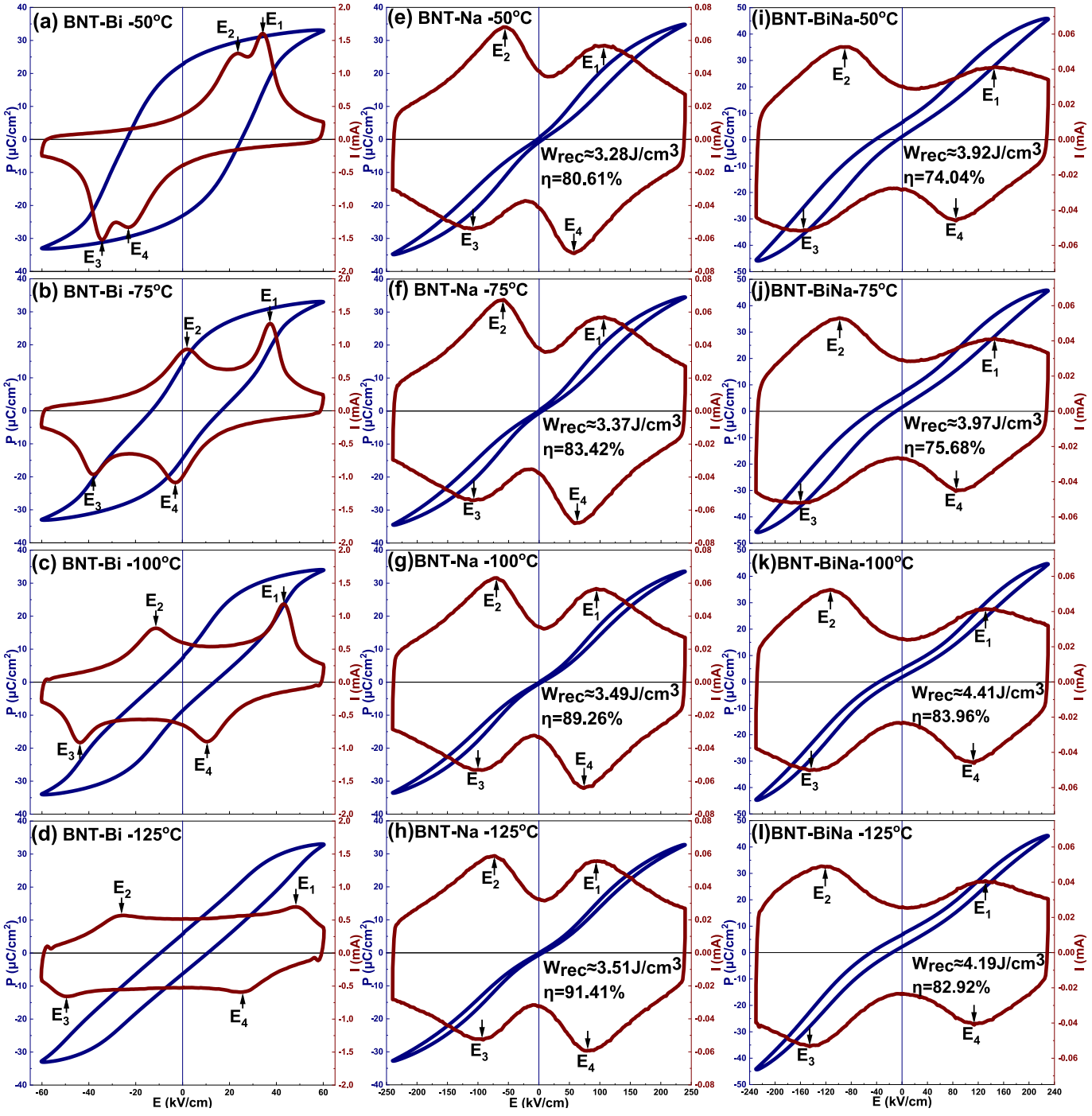

Fig. 5. *P-E* and *I-E* loops of the ceramics of (a-d) BNT-Bi, (e-h) BNT-Na, and (i-l) BNT-BiNa at 50, 75, 100 and 125 °C.

The values of W_{rec} and η for the BNT-Na and BNT-BiNa ceramics were calculated using the Formulae 2 and 3, respectively. At room temperature, the BNT-Na sample showed the maximum W_{rec} of about 3.18 J cm^{-3} and η of about 69.30% at the applied field of 260 kV cm^{-1}. At 240 kV cm^{-1}, the energy storage efficiency of the ceramic is even higher ($\eta \sim$ 71.72%), and the value of W_{rec} is also relatively high (~2.93 J cm^{-3}). For the BNT-BiNa composition, the maximum room-temperature values of W_{rec} of 3.73 J cm^{-3} and η of 62.92% were obtained at 230 kV cm^{-1}. The unipolar *P-E* loops are presented in Fig. S11 (in Supporting Information), showing slightly lower values of the energy storage density compared to these obtained from the bipolar *P-E* loops. The small difference in the calculated W_{rec} values can be attributed to reversibility of the field-induced transitions during bipolar loading. [58,59].

Fig. 5 shows the thermal evolution of the *P-E* and *I-E* loops of the BNT-Bi, BNT-Na, and BNT-BiNa ceramics, as obtained in the temperature range from 50 °C to 125 °C. From Fig. 5(a), one can see that the remanent polarization of BNT-Bi at 50 °C is smaller (~22.75 μC cm^{-2}) than that at room temperature (~25.88 μC cm^{-2}). Besides that, four current peaks are clearly distinguished in the first quadrant and the third quadrant (E_1, E_2, E_3, and E_4) of the *I-E* loop at 50 °C, which is consistent with depolarization process indicated by decrease of d_{33}. The thermally-induced depolarization justifies the degradation of the piezoelectric d_{33} coefficient of the BNT-Bi sample on heating, as mentioned above. With increasing temperature, the E_1 peak gradually shifts towards higher electric fields, and at the same time the gap between the E_1 and E_2 peaks increases. This behaviour suggests a phase transition in the material on heating. Concurrently, the shape of the *P-E* loop changes, the loop becomes slimmer.

As can be in Fig. 5(e) – Fig. 5(h), the difference between the current peaks E_1 and E_4 on the *I-E* curves of the BNT-Na sample gradually decreases with increasing temperature, resulting in the slim *P-E* loop and superior energy storage properties. At 125 °C, the difference between the E_1 and E_4 peaks is the smallest and the energy storage efficiency reaches its maximum (η = 91.41%). At the same time, the remanent polarization decreases upon heating, especially when the temperature is higher than T_d (~64 °C). Unlike the remanent polarization, the saturated polarization does not change significantly with temperature. Therefore, the *P-E* loops become slimmer as the temperature increases. Above 125 °C, the *P-E* loop is wider than that recorded at lower temperatures, which is demonstrated in Fig. S12(b) (in Supporting Information).

The *P-E* and *I-E* loops of the BNT-BiNa ceramic, as collected at temperatures from 50 °C to 125 °C, are shown in Fig. 5(i) – Fig. 5(l). At 50 °C, the distance between the E_1 current peak and the E_4 peak is large, leading to a low energy storage efficiency (η = 74.04%). As the temperature increases, the distance between the E_1 and E_4 peaks decreases. The same trend is observed in the thermal evolution of the remanent polarization, which causes narrowing of the *P-E* loops and enhancement of the energy storage efficiency. However, when the temperature is higher than 100 °C, the remanent polarization increases with temperature and the area of *P-E* loops becomes bigger, which indicate higher losses.

In Fig. 5(b) and Fig. 5(c), the current value between E_1 and E_2 in the first quadrant is higher than that at the highest applied field, which can be related to the decreased domain wall density under high field and field-induced irreversible transitions as well. [60] The reduced density of domain walls is clearly manifested in Fig. 3(a) at temperatures below T_d. As one can see in Fig. 5(f), 5(g), 5(j) and 5(k), the current value between E_1 and E_2 is close to that at the highest field, implying that in the BNT-Na and BNT-BiNa ceramics the field-induced transitions above T_d (Fig. 3(b) and Fig. 3(c)) are reversible. [42,61,62].

The calculated values of W_{rec} and η for the BNT-Na and BNT-BiNa ceramics as a function of temperature are shown in Fig. 6. Apparently, the samples have a relatively high storage performance over a wide temperature range. In Fig. 6(a), one can see that W_{rec} slightly increases from 2.93 J cm^{-3} to 3.51 J cm^{-3} and η increases from 71.72% to 91.41% as the temperature of the BNT-Na sample increases from room temperature up to 125 °C. With further heating to 150 °C, both W_{rec} and η decrease to a certain extent (W_{rec} = 3.20 J cm^{-3} and η = 89.25% at 150 °C).

TEM studies on relaxor ferroelectrics derived from BNT have shown that these materials are composed of ferroelectric micro-domains and polar nanoregions (PNRs). [33,57,63] The PNRs have been demonstrated to be responsible for the electric field-induced phase transition above T_d. This transition is reversible under an external switching field and is typically manifested by four electrical current peaks in the four quadrants of the *I-E* curve. [42,64] In Fig. 5, one can clearly observe the four current peaks for BNT-BiNa at 100 °C. Moreover, the fields corresponding to the current peaks E_1 and E_4 are very close to each other, which indicates a high performance of BNT-BiNa for storage of energy at temperatures as high as 100 °C.

Fig. 6(b) shows the temperature dependence of W_{rec} and η of the BNT-BiNa sample under an applied field of 230 kV cm^{-1}. Similar to the BNT-Na ceramic, the BNT-BiNa sample has the lowest values of W_{rec} and η at room temperature. Due to the relatively wide *P-E* loop (Fig. 4(c)), the room temperature η is lower than that of the BNT-Na, reaching the value ~ 62.92%. However, the high saturated polarization of BNT-BiNa yields a higher W_{rec} (≈ 3.73 J cm^{-3}) at room temperature, if compared to the value of the recoverable energy storage density of the BNT-Na

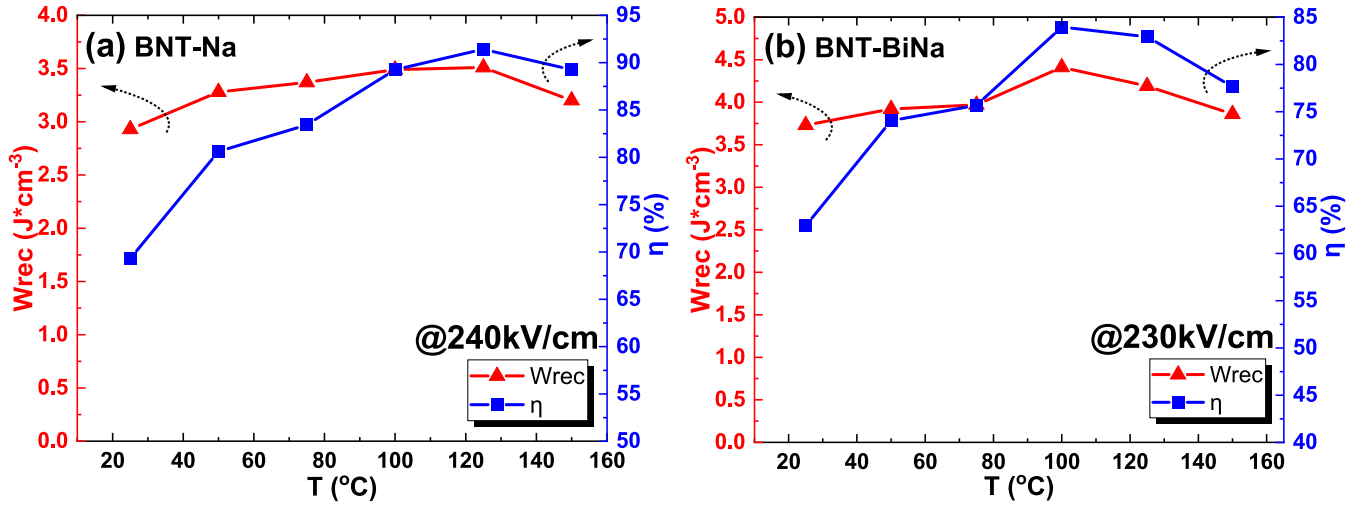

Fig. 6. The recoverable energy storage density (W_{rec}) and energy storage efficiency (η) as function of temperature for (a) BNT-Na (at 240 kV cm^{-1}), and (b) BNT-BiNa (at 230 kV cm^{-1}).

sample. As the temperature increases, W_{rec} and η increase, with a steep rise at a temperature around 75 °C, followed by the peak values of W_{rec} = 4.41 J cm^{-3} and η = 83.96% at 100 °C. Further increasing of the temperature leads to a slow decreasing of W_{rec} and η; the respective values dropped down to 3.86 J cm^{-3} and 77.65% at 150 °C. It is worth mentioning that at 125 °C the values of W_{rec} and η are yet as high as 4.19 J cm^{-3} and 82.92%, respectively. The energy storage properties of the BNT-Na and BNT-BiNa ceramics are summarized in Table S2 (in Supporting Information).

From the obtained results, it can be postulated that the magnitude of W_{rec} depends on energy storage material's parameters, such as the remanent polarization, the saturated polarization, and the breakdown electric field strength. Among them, the remanent and saturation polarizations are intrinsic characteristics of the material. Upon electric field loading, the saturation polarization increases very little. Therefore, to obtain a larger W_{rec} a larger breakdown electric field strength of the ferroelectric materials is required. Bulk ceramics is often grounded and polished to a very small thickness in order to achieve a large electric field at a given working voltage. However, due to low capacity and small volume, the total energy that can be stored in the thin ceramics is much lower than that in their bulk counterparts. In addition, large external electric fields applied to naturally non-perfect polycrystalline ceramics are not safe in practical use. [65,66] Therefore, the search for novel materials that do not require extremely large electric fields to show high recoverable energy storage density and efficiency is important and challenging in modern material sciences.

Here, we propose a new concept for an assessment of energy storage materials based on determining the energy density under a certain electric field; the so-called recoverable energy storage intensity (ρ). The recoverable energy storage intensity (ρ) can be calculated using the following formulae:

$$\rho = \frac{W_{rec}}{\Delta E} \tag{4}$$

$$\Delta E = E_b - E_s \tag{5}$$

where E_b is the breakdown electric field and E_s is the starting electric field, which is normally defined as 0 kV cm^{-1}. From the Formula 5, if E_s = 0 kV cm^{-1}, ΔE equals to the breakdown electric field. In our study, the calculated room-temperature value of ρ for the BNT-Na and BNT-BiNa ceramics is 12.23 × 10^{-3} J kV^{-1} cm^{-2} and 16.22 × 10^{-3} J kV^{-1} cm^{-2}, respectively. The maximum recoverable energy storage intensity (ρ_{max} = 14.63 × 10^{-3} J kV^{-1} cm^{-2}) of the BNT-Na sample was obtained at 125 °C. The BNT-BiNa sample showed the maximal ρ of about 19.17 × 10^{-3} J kV^{-1} cm^{-2} at lower temperature, around 100 °C, which is the highest value of the recoverable energy storage intensity obtained for the relaxor-based ceramics so far. It should be emphasized that all over the investigated temperature range from 25 °C to 150 °C the ρ values of the two ceramics (BNT-Na and BNT-BiNa) are higher than 12 × 10^{-3} J

Table 2
The energy storage properties of ferroelectric ceramics.

Compound[a)]	$\triangle E$ (kV cm^{-1})	W_{rec} (J cm^{-3})	η (%)	ρ (J kV^{-1} cm^{-2})	Temperature (℃) [b)]	Ref.
0.70BT-0.30BS	730	6.1	- [c)]	8.36 × 10^{-3}	RT	[67]
BNBT-0.06KN	100	0.89	–	8.90 × 10^{-3}	RT	[68]
0.97(0.65BF-0.35BT)-0.03Nb_2O_5	90	0.71	–	7.89 × 10^{-3}	–	[69]
0.70(0.94BNT-0.06BT)-0.30ST	90	0.98	82	10.89 × 10^{-3}	RT	[70]
0.88BT-0.12BMT	224	1.81	–	8.08 × 10^{-3}	RT	[71]
0.85BT-0.15BZT (MLCC)	330	2.8	–	8.48 × 10^{-3}	RT	[72]
0.91BT-0.09BY	93	0.71	82.6	7.63 × 10^{-3}	RT	[73]
0.90BT-0.10BMN	143.5	1.13	> 90	7.87 × 10^{-3}	RT	[74]
0.80(0.92BNT-0.08BT)-0.20NBN	136	1.36	73.9	10.00 × 10^{-3}	–	[75]
0.61BF-0.33BT-0.06BaMN	125	1.56	75	12.48 × 10^{-3}	RT	[76]
BBNT-0.15SZ	155	1.32	~ 56	8.52 × 10^{-3}	–	[77]
0.90(0.92BNT-0.08BT)-0.10BMT	135	2	88	14.81 × 10^{-3}	120℃	[78]
0.80KNN-0.20SSN	295	2.02	81.4	6.85 × 10^{-3}	RT	[79]
0.80KNN-0.20SSN-0.5 %ZnO	400	2.6	73.2	6.50 × 10^{-3}	RT	[80]
0.85BT-0.15BZN	131	0.79	93.5	6.03 × 10^{-3}	–	[81]
0.90(0.92BNT-0.08BT)-0.10NT	100	1.2	74.8	12.00 × 10^{-3}	RT	[82]
0.85KNN-0.15ST	400	4.03	52	10.08 × 10^{-3}	RT	[83]
0.80KNN-0.20ST	400	3.67	72.1	9.18 × 10^{-3}	RT	[83]
0.90KNN-0.10BMeN	300	4.08	62.7	13.60 × 10^{-3}	RT	[84]
0.90LLBNTZ-0.10NBN	178	2.04	54.76	11.46 × 10^{-3}	RT	[85]
0.61BF-0.33BT-0.06LMT	130	1.66	82	12.77 × 10^{-3}	RT	[86]
$Sr_{0.30}(Bi_{0.70}Na_{0.67}Li_{0.03})_{0.5}TiO_3$	130	1.70	87.2	13.08 × 10^{-3}	RT	[57]
0.85BT-0.15BZS	280	2.21	91.6	7.89 × 10^{-3}	RT	[87]
0.60BKT-0.30BT-0.10NN	460	7.57	81.4	16.46 × 10^{-3}	RT	[88]
0.94(0.95BNT-0.04BT)-0.06BZN	210	3.02	75	14.38 × 10^{-3}	–	[89]
0.90NN-0.10BF	995	18.5	78.7	18.59 × 10^{-3}	–	[65]
0.68NN-0.32BLT	485	8.73	80.1	18.00 × 10^{-3}	RT	[16]
0.35BF-0.65ST	750	8.4	90	11.20 × 10^{-3}	–	[66]
0.62BF-0.3BT-0.08NZZ (MLCC)	700	10.5	87	15.00 × 10^{-3}	25℃	[15]
0.45$AgNbO_3$–0.55$AgTaO_3$	470	6.3	90	13.40 × 10^{-3}	–	[13]
$Ag_{0.76}La_{0.08}NbO_3$	476	7.01	77	14.73 × 10^{-3}	RT	[90]
KNN-H (high-entropy)	740	10.06	90.8	13.59 × 10^{-3}	–	[91]
BNT-Na	**260**	**3.18**	**69.30**	**12.23 × 10^{-3}**	**RT**	**This work**
BNT-Na	**240**	**3.51**	**91.41**	**14.63 × 10^{-3}**	**125℃**	**This work**
BNT-BiNa	**230**	**3.73**	**62.92**	**16.22 × 10^{-3}**	**RT**	**This work**
BNT-BiNa	**230**	**4.41**	**83.96**	**19.17 × 10^{-3}**	**100℃**	**This work**

[a)] BT: $BaTiO_3$; BS: $BiScO_3$; BNBT: $(Bi_{0.47}Na_{0.47}Ba_{0.06})TiO_3$; KN: $KNbO_3$; BF: $BiFeO_3$; BNT: $(Bi_{0.5}Na_{0.5})TiO_3$; ST: $SrTiO_3$; BMT: $Bi(Mg_{0.5}Ti_{0.5})O_3$; BZT: $Bi(Zn_{0.5}Ti_{0.5})O_3$; BY: $BiYbO_3$; BMN: $Bi(Mg_{2/3}Nb_{1/3})O_3$; NBN: $Na_{0.73}Bi_{0.09}NbO_3$; BaMN: $Ba(Mg_{1/3}Nb_{2/3})O_3$; BBNT: $Ba_{0.04}Bi_{0.48}Na_{0.48}TiO_3$; SZ: $SrZrO_3$; KNN: $(K_{0.5}Na_{0.5})NbO_3$; SSN: $Sr(Sc_{0.5}Nb_{0.5})O_3$; BZN: $Bi(Zn_{2/3}Nb_{1/3})O_3$; NT: $NaTaO_3$; LLBNTZ: $Bi_{0.48}La_{0.02}Na_{0.48}Li_{0.02}Ti_{0.98}Zr_{0.02}O_3$; BMeN: $Bi(Me_{2/3}Nb_{1/3})O_3$; LMT: $La(Mg_{0.5}Ti_{0.5})O_3$; BNLT: $(Bi_{0.5}Na_{0.485}Li_{0.015})TiO_3$; BZS: $Bi(Zn_{1/2}Sn_{1/2})O_3$; BKT: $(Bi_{0.5}K_{0.5})TiO_3$; NN:$NaNbO_3$; BLT: $(Bi_{0.5}Li_{0.5})TiO_3$; NZZ: $Nd(Zn_{0.5}Zr_{0.5})O_3$; KNN-H: $[(K_{0.2}Na_{0.8})_{0.8}Li_{0.08}Ba_{0.02}Bi_{0.1}](Nb_{0.68}Sc_{0.02}Hf_{0.08}Zr_{0.1}Ta_{0.08}Sb_{0.04})O_3$.

[b)] RT: Room Temperature.

[c)] "-": data not provided.

kV^{-1} cm^{-2}. Table 2 summarizes and compares the energy storage properties of the BNT-Na and BNT-BiNa ceramics with other recently developed ceramic materials for high performance energy storage applications.

Obviously, some materials listed in the table have larger W_{rec} than the Sm-doped BNT-6BT ceramics. However, higher W_{rec} values are due to higher applied electric fields. If one compares the values of the recoverable energy storage intensities, none of the listed materials show higher or comparable values to that achieved in this study (19.17×10^{-3} J kV^{-1} cm^{-2}). Also, it should be noted that BKT-based and NN-based ceramics show better energy storage properties than the prepared Sm-doped BNT-6BT ceramics. The higher values of the W_{rec}, η and ρ parameters of the ceramics derived from BKT and NN can be attributed to the high field-induced polarization. [16,65,88].

4. Conclusion

The Sm-doped BNT-6BT ceramics were prepared by conventional solid-state reaction. The composition of the ceramics was designed to replace Bi, Na and both Bi and Na ions by Sm ions in the BNT-6BT perovskite system. The effect of the Sm substitution on the crystal structure, dielectric, ferroelectric and piezoelectric properties as well as energy storage properties of the ceramics was investigated systematically. It is shown that the BNT-Bi (Sm replaces Bi) sample shows good piezoelectric properties ($d_{33} = \pm 117.3$ pC N^{-1}) and adequate ferroelectric properties with the large remanent polarization (25.88 μC cm^{-2}) at room temperature.

The BNT-Na (Sm replaces Na) and BNT-BiNa (Sm ions replace both the Bi and Na ions) ceramics exhibit superior energy storage properties due to their relaxor behaviour. The ultrahigh recoverable energy storage density (4.41 J cm^{-3}), excellent energy storage efficiency (83.96%) and superhigh recoverable energy storage intensity (19.17×10^{-3} J kV^{-1} cm^{-2}) were achieved simultaneously in the BNT-BiNa ceramic. In addition, a notable thermal stability of the energy storage performance was observed for the BNT-Na and BNT-BiNa ceramics. In the temperature range 25 °C – 150 °C, the recoverable energy storage densities and recoverable energy storage intensities of these samples were about 3 J cm^{-3} and 12×10^{-3} J kV^{-1} cm^{-2}, respectively, and they did not change significantly with temperature. This research provides an approach, based on simple but reasonable chemical modifications of BNT-6BT relaxor ferroelectrics, for the development of new lead-free ceramics for piezoelectric and energy storage applications.

Declaration of Competing Interest

The authors declare that they have no known competing financial interests or personal relationships that could have appeared to influence the work reported in this paper.

Data availability

Data will be made available on request.

Acknowledgements

This work was supported by the Royal Society grant (NAF\R1 \201126), Grant Agency of the Slovak Academy of Sciences (VEGA Grant No. 2/0034/23), and China Scholarship Council (No. 202006040021). Dr. E. Mudra is greatly acknowledged for her assistance in Raman spectroscopy of samples.

Appendix A. Supplementary data

Supplementary data to this article can be found online at https://doi.org/10.1016/j.cej.2023.145363.

References

[1] International Energy Agency (IEA), Key World Energy Statistics 2021. https://www.iea.org/reports/key-world-energy-statistics-2021, Paris, 2021.
[2] A. Evans, V. Strezov, T.J. Evans, Assessment of utility energy storage options for increased renewable energy penetration, Renew. Sustain. Energy Rev. 16 (2012) 4141–4147, https://doi.org/10.1016/j.rser.2012.03.048.
[3] H. Ibrahim, A. Ilinca, J. Perron, Energy storage systems—Characteristics and comparisons, Renew. Sustain. Energy Rev. 12 (5) (2008) 1221–1250, https://doi.org/10.1016/j.rser.2007.01.023.
[4] C. Liu, F. Li, L.P. Ma, H.M. Cheng, Advanced materials for energy storage, Adv Mater 22 (8) (2010) E28–E62, https://doi.org/10.1002/adma.200903328.
[5] A.G. Olabi, Energy quadrilemma and the future of renewable energy, Energy 108 (2016) 1–6, https://doi.org/10.1016/j.energy.2016.07.145.
[6] B. Chu, X. Zhou, K. Ren, B. Neese, M. Lin, Q. Wang, F. Bauer, Q. Zhang, A dielectric polymer with high electric energy density and fast discharge speed, Science 313 (5785) (2006) 334–336, https://doi.org/10.1126/science.1127798.
[7] Q.i. Li, L. Chen, M.R. Gadinski, S. Zhang, G. Zhang, H.U. Li, E. Iagodkine, A. Haque, L.-Q. Chen, T.N. Jackson, Q. Wang, Flexible high-temperature dielectric materials from polymer nanocomposites, Nature 523 (7562) (2015) 576–579.
[8] L. Yang, X. Kong, F. Li, H. Hao, Z. Cheng, H. Liu, J.-F. Li, S. Zhang, Perovskite lead-free dielectrics for energy storage applications, Prog. Mater Sci. 102 (2019) 72–108, https://doi.org/10.1016/j.pmatsci.2018.12.005.
[9] B. Yang, Y. Zhang, H. Pan, W. Si, Q. Zhang, Z. Shen, Y. Yu, S. Lan, F. Meng, Y. Liu, H. Huang, J. He, L. Gu, S. Zhang, L.-Q. Chen, J. Zhu, C.-W. Nan, Y.-H. Lin, High-entropy enhanced capacitive energy storage, Nat. Mater. 21 (9) (2022) 1074–1080, https://doi.org/10.1038/s41563-022-01274-6.
[10] H. Pan, F. Li, Y. Liu, Q. Zhang, M. Wang, S. Lan, Y. Zheng, J. Ma, L. Gu, Y. Shen, P. Yu, S. Zhang, L.-Q. Chen, Y.-H. Lin, C.-W. Nan, Ultrahigh-energy density lead-free dielectric films via polymorphic nanodomain design, Science 365 (6453) (2019) 578–582, https://doi.org/10.1126/science.aaw8109.
[11] L. Zhao, Q. Liu, J. Gao, S. Zhang, J.F. Li, Lead-Free Antiferroelectric Silver Niobate Tantalate with High Energy Storage Performance, Adv Mater 29 (2017) 1701824, https://doi.org/10.1002/adma.201701824.
[12] J. Li, F. Li, Z. Xu, S. Zhang, Multilayer Lead-Free Ceramic Capacitors with Ultrahigh Energy Density and Efficiency, Adv Mater 30 (32) (2018) 1802155, https://doi.org/10.1002/adma.201802155.
[13] N. Luo, K. Han, M.J. Cabral, X. Liao, S. Zhang, C. Liao, G. Zhang, X. Chen, Q. Feng, J.F. Li, Y. Wei, Constructing phase boundary in $AgNbO_3$ antiferroelectrics: pathway simultaneously achieving high energy density and efficiency, Nat Commun 11 (1) (2020) 4824, https://doi.org/10.1038/s41467-020-18665-5.
[14] J. Li, Z. Shen, X. Chen, S. Yang, W. Zhou, M. Wang, L. Wang, Q. Kou, Y. Liu, Q. Li, Z. Xu, Y. Chang, S. Zhang, F. Li, Grain-orientation-engineered multilayer ceramic capacitors for energy storage applications, Nat Mater 19 (9) (2020) 999–1005, https://doi.org/10.1038/s41563-020-0704-x.
[15] G. Wang, J. Li, X. Zhang, Z. Fan, F. Yang, A. Feteira, D. Zhou, D.C. Sinclair, T. Ma, X. Tan, D. Wang, I.M. Reaney, Ultrahigh energy storage density lead-free multilayers by controlled electrical homogeneity, Energ. Environ. Sci. 12 (2) (2019) 582–588, https://doi.org/10.1039/C8EE03287D.
[16] A. Xie, R. Zuo, Z. Qiao, Z. Fu, T. Hu, L. Fei, NaNbO3-(Bi0.5Li0.5)TiO3 Lead-Free Relaxor Ferroelectric Capacitors with Superior Energy-Storage Performances via Multiple Synergistic Design, Adv. Energy Mater. 11 (28) (2021) 2101378, https://doi.org/10.1002/aenm.202101378.
[17] T. Takenaka, K.-I. Kei-ichi Maruyama, K.S. Koichiro Sakata, (Bi1/2Na1/2)TiO3-BaTiO3 system for lead-free piezoelectric ceramics, Jpn. J. Appl. Phys. 30 (9S) (1991) 2236.
[18] G. Viola, Y. Tian, C. Yu, Y. Tan, V. Koval, X. Wei, K.-L. Choy, H. Yan, Electric field-induced transformations in bismuth sodium titanate-based materials, Prog. Mater Sci. 122 (2021), 100837, https://doi.org/10.1016/j.pmatsci.2021.100837.
[19] F. Li, D. Lin, Z. Chen, Z. Cheng, J. Wang, C. Li, Z. Xu, Q. Huang, X. Liao, L.Q. Chen, T.R. Shrout, S. Zhang, Ultrahigh piezoelectricity in ferroelectric ceramics by design, Nat Mater 17 (4) (2018) 349–354, https://doi.org/10.1038/s41563-018-0034-4.
[20] F. Li, M.J. Cabral, B. Xu, Z. Cheng, E.C. Dickey, J.M. LeBeau, J. Wang, J. Luo, S. Taylor, W. Hackenberger, L. Bellaiche, Z. Xu, L.-Q. Chen, T.R. Shrout, S. Zhang, Giant piezoelectricity of Sm-doped Pb (Mg1/3Nb2/3) O3-PbTiO3 single crystals, Science 364 (6437) (2019) 264–268.
[21] B. Malic, T. Rojac, High piezoelectricity via enhanced disorder, Nat. Mater. 17 (4) (2018) 297–298, https://doi.org/10.1038/s41563-018-0046-0.
[22] Q. Guo, F. Li, F. Xia, X. Gao, P. Wang, H. Hao, H. Sun, H. Liu, S. Zhang, High-Performance Sm-Doped Pb(Mg1/3Nb2/3)O3 - PbZrO3 - PbTiO3 - Based Piezoceramics, ACS Appl Mater Interfaces 11 (46) (2019) 43359–43367, https://doi.org/10.1021/acsami.9b15424.
[23] R.D. Shannon, Revised effective ionic radii and systematic studies of interatomic distances in halides and chalcogenides, Acta Crystallogr. Sect. A: Cryst. Phys., Diffr., Theor. Gen. Crystallogr. 32 (5) (1976) 751–767, https://doi.org/10.1107/S0567739476001551.
[24] A. Mahajan, H. Zhang, J. Wu, E. Venkata Ramana, C. Yu, N.V. Tarakina, M. J. Reece, H. Yan, Effect of processing on the structures and properties of bismuth sodium titanate compounds, J. Mater. Res. 36 (2021) 1195–1205, https://doi.org/10.1557/s43578-020-00040-1.
[25] M. Zhang, X. Xu, Y. Yue, M. Palma, M.J. Reece, H. Yan, Multi elements substituted Aurivillius phase relaxor ferroelectrics using high entropy design concept, Mater. Des. 200 (2021), 109447, https://doi.org/10.1016/j.matdes.2020.109447.
[26] M. Zhang, H. Zhang, Q. Jiang, F. Gao, R. Chen, D. Zhang, M.J. Reece, B. Yang, G. Viola, H. Yan, Terahertz Characterization of Lead-Free Dielectrics for Different

Applications, ACS Appl Mater Interfaces 13 (2021) 53492–53503, https://doi.org/10.1021/acsami.1c14583.
[27] N. Meng, X. Ren, X. Zhu, J. Wu, B. Yang, F. Gao, H. Zhang, Y. Liao, E. Bilotti, M. J. Reece, H. Yan, Multiscale understanding of electric polarization in poly (vinylidene fluoride)-based ferroelectric polymers, J. Mater. Chem. C 8 (2020) 16436–16442, https://doi.org/10.1039/D0TC04310A.
[28] M. Zhang, Z. Chen, Y. Yue, T. Chen, Z. Yan, Q. Jiang, B. Yang, M. Eriksson, J. Tang, D. Zhang, Z. Shen, I. Abrahams, H. Yan, Terahertz Reading of Ferroelectric Domain Wall Dielectric Switching, ACS Appl Mater Interfaces 13 (10) (2021) 12622–12628, https://doi.org/10.1021/acsami.1c00523.
[29] B.-J. Chu, D.-R. Chen, G.-R. Li, Q.-R. Yin, Electrical properties of $Na_{1/2}Bi_{1/2}TiO_3$–$BaTiO_3$ ceramics, J. Eur. Ceram. Soc. 22 (2002) 2115–2121, https://doi.org/10.1016/S0955-2219(02)00027-4.
[30] M. Chen, Q. Xu, B.H. Kim, B.K. Ahn, J.H. Ko, W.J. Kang, O.J. Nam, Structure and electrical properties of (Na0.5Bi0.5)1−xBaxTiO3 piezoelectric ceramics, J. Eur. Ceram. Soc. 28 (2008) 843–849, https://doi.org/10.1016/j.jeurceramsoc.2007.08.007.
[31] S.-T. Zhang, A.B. Kounga, E. Aulbach, Y. Deng, Temperature-Dependent Electrical Properties of $0.94Bi_{0.5}Na_{0.5}TiO_3$-$0.06BaTiO_3$ Ceramics, J. Am. Ceram. Soc. 91 (12) (2008) 3950–3954, https://doi.org/10.1111/j.1551-2916.2008.02778.x.
[32] C. Ma, H. Guo, S.P. Beckman, X. Tan, Creation and destruction of morphotropic phase boundaries through electrical poling: a case study of lead-free (Bi1/2Na1/2)TiO3-BaTiO3 piezoelectrics, Phys Rev Lett 109 (10) (2012), 107602, https://doi.org/10.1103/PhysRevLett.109.107602.
[33] C. Ma, X. Tan, E. Dul'kin, M. Roth, Domain structure-dielectric property relationship in lead-free $(1-x)(Bi_{1/2}Na_{1/2})TiO_3$-$xBaTiO_3$ ceramics, Journal of Applied Physics 108(10) (2010) 104105. https://doi.org/10.1063/1.3514093.
[34] E.-M. Anton, W. Jo, D. Damjanovic, J. Rödel, Determination of depolarization temperature of $(Bi_{1/2}Na_{1/2})TiO_3$-based lead-free piezoceramics, Journal of Applied Physics 110 (2011) 094108. https://doi.org/10.1063/1.3660253.
[35] G. Viola, H. Ning, X. Wei, M. Deluca, A. Adomkevicius, J. Khaliq, M. John Reece, H. Yan, Dielectric relaxation, lattice dynamics and polarization mechanisms in $Bi_{0.5}Na_{0.5}TiO_3$-based lead-free ceramics, Journal of Applied Physics 114(1) (2013) 014107. https://doi.org/10.1063/1.4812383.
[36] Y. Hiruma, H. Nagata, T. Takenaka, Phase diagrams and electrical properties of $(Bi_{1/2}Na_{1/2})TiO_3$-based solid solutions, Journal of Applied Physics 104(12) (2008) 124106. https://doi.org/10.1063/1.3043588.
[37] A.A. Bokov, Z.G. Ye, Recent progress in relaxor ferroelectrics with perovskite structure, J. Mater. Sci. 41 (1) (2006) 31–52, https://doi.org/10.1007/s10853-005-5915-7.
[38] R. Garg, B.N. Rao, A. Senyshyn, P.S.R. Krishna, R. Ranjan, Lead-free piezoelectric system (Na0.5Bi0.5)TiO3-BaTiO3: Equilibrium structures and irreversible structural transformations driven by electric field and mechanical impact, Phys. Rev. B 88 (1) (2013), 014103. https://link.aps.org/doi/10.1103/PhysRevB.88.014103.
[39] D. Damjanovic, N. Klein, J.I.N. Li, V. Porokhonskyy, What Can Be Expected from Lead-Free Piezoelectric Materials? Funct. Mater. Lett. 03 (01) (2010) 5–13, https://doi.org/10.1142/S1793604710000919.
[40] M. Barsoum, Fundamentals of ceramics, second ed., CRC Press, Boca Raton, 2019.
[41] O. Bidault, P. Goux, M. Kchikech, M. Belkaoumi, M. Maglione, Space-charge relaxation in perovskites, Phys. Rev. B 49 (12) (1994) 7868. https://link.aps.org/doi/10.1103/PhysRevB.49.7868.
[42] G. Viola, R. Mkinnon, V. Koval, A. Adomkevicius, S. Dunn, H. Yan, Lithium-Induced Phase Transitions in Lead-Free $Bi_{0.5}Na_{0.5}TiO_3$ Based Ceramics, J. Phys. Chem. C 118 (2014) 8564–8570, https://doi.org/10.1021/jp500609h.
[43] N.B. Mahmood, E.K. Al-Shakarchi, Dielectric properties of BNT-xBT prepared by hydrothermal process, J. Adv. Dielectr. 07 (03) (2017) 1750019, https://doi.org/10.1142/S2010135X17500199.
[44] W. Hu, Y. Liu, R.L. Withers, T.J. Frankcombe, L. Noren, A. Snashall, M. Kitchin, P. Smith, B. Gong, H. Chen, J. Schiemer, F. Brink, J. Wong-Leung, Electron-pinned defect-dipoles for high-performance colossal permittivity materials, Nat Mater 12 (9) (2013) 821–826, https://doi.org/10.1038/nmat3691.
[45] Z.-T. Li, H. Liu, H.-C. Thong, Z. Xu, M.-H. Zhang, J. Yin, J.-F. Li, K. Wang, J. Chen, Enhanced Temperature Stability and Defect Mechanism of BNT-Based Lead-Free Piezoceramics Investigated by a Quenching Process, Adv. Electron. Mater. 5 (3) (2019) 1800756, https://doi.org/10.1002/aelm.201800756.
[46] X. Zhang, J. Qin, Y. Xue, P. Yu, B. Zhang, L. Wang, R. Liu, Effect of aspect ratio and surface defects on the photocatalytic activity of ZnO nanorods, Sci Rep 4 (2014) 4596, https://doi.org/10.1038/srep04596.
[47] E. Ramos-Moore, P. Ferrari, D.E. Diaz-Droguett, D. Lederman, J.T. Evans, Raman and x-ray photoelectron spectroscopy study of ferroelectric switching in Pb(Nb,Zr,Ti)O_3 thin films, Journal of Applied Physics 111(1) (2012) 014108. https://doi.org/10.1063/1.3675479.
[48] D. Damjanovic, Ferroelectric, dielectric and piezoelectric properties of ferroelectric thin films and ceramics, Rep. Prog. Phys. 61 (9) (1998) 1267, https://doi.org/10.1088/0034-4885/61/9/002.
[49] B. Jaffe, W. Cook, H. Jaffe, Piezoelectric Ceramics, first ed., Academic Press, London, 1971.
[50] J. Wu, Perovskite lead-free piezoelectric ceramics, J. Appl. Phys. 127 (19) (2020), 190901, https://doi.org/10.1063/5.0006261.
[51] I. Jeong, C.Y. Park, D.J. Kim, S.-h. Kim, B.K. Moon, I.W. Kim, C.W. Ahn, Neutron total scattering studies on A-site disorder in lead-free ferroelectric $Bi_{0.5}(Na_{1-x}K_x)_{0.5}TiO_3$, 226(2) (2011) 150-154. https://doi.org/10.1524/zkri.2011.1295.
[52] E. Aksel, J.S. Forrester, J.C. Nino, K. Page, D.P. Shoemaker, J.L. Jones, Local atomic structure deviation from average structure of $Na_{0.5}Bi_{0.5}TiO_3$: Combined x-ray and neutron total scattering study, Phys. Rev. B 87 (10) (2013), 104113. https://link.aps.org/doi/10.1103/PhysRevB.87.104113.
[53] J. Kling, X. Tan, W. Jo, H.-J. Kleebe, H. Fuess, J. Rödel, In Situ Transmission Electron Microscopy of Electric Field-Triggered Reversible Domain Formation in Bi-Based Lead-Free Piezoceramics, J. Am. Ceram. Soc. 93 (9) (2010) 2452–2455, https://doi.org/10.1111/j.1551-2916.2010.03778.x.
[54] H. Zhang, H. Yan, H. Ning, M.J. Reece, M. Eriksson, Z. Shen, Y. Kan, P. Wang, The grain size effect on the properties of Aurivillius phase $Bi_{3.15}Nd_{0.85}Ti_3O_{12}$ ferroelectric ceramics, Nanotechnology 20 (38) (2009), 385708, https://doi.org/10.1088/0957-4484/20/38/385708.
[55] M. Waqar, H. Wu, J. Chen, K. Yao, J. Wang, Evolution from Lead-Based to Lead-Free Piezoelectrics: Engineering of Lattices, Domains, Boundaries, and Defects Leading to Giant Response, Adv Mater 34 (25) (2021) 2106845, https://doi.org/10.1002/adma.202106845.
[56] L.E. Cross, Relaxorferroelectrics: An overview, Ferroelectrics 151 (1) (1994) 305–320, https://doi.org/10.1080/00150199408244755.
[57] J. Wu, A. Mahajan, L. Riekehr, H. Zhang, B. Yang, N. Meng, Z. Zhang, H. Yan, Perovskite Srx(Bi1−xNa0.97−xLi0.03)0.5TiO3 ceramics with polar nano regions for high power energy storage, Nano Energy 50 (2018) 723–732, https://doi.org/10.1016/j.nanoen.2018.06.016.
[58] V.Y. Shur, E.L. Rumyantsev, G.G. Lomakin, O.V. Yakutova, D.V. Pelegov, A. Sternberg, M. Kosec, Field Induced Evolution of Nanoscale Structures in Relaxor PLZT Ceramics, Ferroelectrics 316 (2005) 23–29, https://doi.org/10.1080/00150190590963093.
[59] X.J. Lou, J. Wang, Bipolar and unipolar electrical fatigue in ferroelectric lead zirconate titanate thin films: An experimental comparison study, Journal of Applied Physics 108 (2010) 034104. https://doi.org/10.1063/1.3463318.
[60] J. Wu, H. Zhang, C.-H. Huang, C.-W. Tseng, N. Meng, V. Koval, Y.-C. Chou, Z. Zhang, H. Yan, Ultrahigh field-induced strain in lead-free ceramics, Nano Energy 76 (2020), 105037, https://doi.org/10.1016/j.nanoen.2020.105037.
[61] M. Zhang, X. Xu, S. Ahmed, Y. Yue, M. Palma, P. Svec, F. Gao, I. Abrahams, M. J. Reece, H. Yan, Phase transformations in an Aurivillius layer structured ferroelectric designed using the high entropy concept, Acta Mater. 229 (2022), 117815, https://doi.org/10.1016/j.actamat.2022.117815.
[62] Z. Yan, D. Zhang, X. Zhou, M. Zhang, Y. Yue, L. Zhang, G. Xue, H. Luo, I. Abrahams, H. Yan, Phase transitions in RbPrNb2O7, a layer structured ferroelectric with a high Curie point, Acta Mater. 200 (2020) 971–979, https://doi.org/10.1016/j.actamat.2020.09.066.
[63] C. Ma, X. Tan, H.J. Kleebe, In situ Transmission Electron Microscopy Study on the Phase Transitionsin Lead-Free (1–x)(Bi1/2Na1/2)TiO3-xBaTiO3 Ceramics, J. Am. Ceram. Soc. 94 (2011) 4040–4044, https://doi.org/10.1111/j.1551-2916.2011.04670.x.
[64] X. Liu, X. Tan, Giant Strains in Non-Textured (Bi1/2Na1/2)TiO3 -Based Lead-Free Ceramics, Adv Mater 28 (2016) 574–578, https://doi.org/10.1002/adma.201503768.
[65] J. Jiang, X. Meng, L. Li, S. Guo, M. Huang, J. Zhang, J. Wang, X. Hao, H. Zhu, S.-T. Zhang, Ultrahigh energy storage density in lead-free relaxor antiferroelectric ceramics via domain engineering, Energy Storage Mater. 43 (2021) 383–390, https://doi.org/10.1016/j.ensm.2021.09.018.
[66] F. Yan, H. Bai, G. Ge, J. Lin, C. Shi, K. Zhu, B. Shen, J. Zhai, S. Zhang, Composition and Structure Optimized $BiFeO_3$ -$SrTiO_3$ Lead-Free Ceramics with Ultrahigh Energy Storage Performance, Small 18 (10) (2022) 2106515, https://doi.org/10.1002/smll.202106515.
[67] H. Ogihara, C.A. Randall, S. Trolier-McKinstry, High-Energy Density Capacitors Utilizing $0.7BaTiO_3$-$0.3BiScO_3$ Ceramics, Journal of the American Ceramic Society 92(8) (2009) 1719-1724. https://doi.org/10.1111/j.1551-2916.2009.03104.x.
[68] B. Wang, L. Luo, X. Jiang, W. Li, H. Chen, Energy-storage properties of (1–x) Bi0.47Na0.47Ba0.06TiO3–xKNbO3 lead-free ceramics, Journal of Alloys and Compounds 585 (2014) 14–18, https://doi.org/10.1016/j.jallcom.2013.09.052.
[69] T. Wang, L. Jin, Y. Tian, L. Shu, Q. Hu, X. Wei, Microstructure and ferroelectric properties of Nb_2O_5-modified $BiFeO_3$-$BaTiO_3$ lead-free ceramics for energy storage, Mater. Lett. 137 (2014) 79–81, https://doi.org/10.1016/j.matlet.2014.08.133.
[70] W. Cao, W. Li, T. Zhang, J. Sheng, Y. Hou, Y. Feng, Y. Yu, W. Fei, High-Energy Storage Density and Efficiency of (1−x)[0.94 NBT-0.06 BT]-xST Lead-Free Ceramics, Energy Technology 3(12) (2015) 1198-1204. https://doi.org/10.1002/ente.201500173.
[71] Q. Hu, L. Jin, T. Wang, C. Li, Z. Xing, X. Wei, Dielectric and temperature stable energy storage properties of 0.88BaTiO3–0.12Bi(Mg1/2Ti1/2)O3 bulk ceramics, Journal of Alloys and Compounds 640 (2015) 416–420, https://doi.org/10.1016/j.jallcom.2015.02.225.
[72] N. Kumar, A. Ionin, T. Ansell, S. Kwon, W. Hackenberger, D. Cann, Multilayer ceramic capacitors based on relaxor $BaTiO_3$-$Bi(Zn_{1/2}Ti_{1/2})O_3$ for temperature stable and high energy density capacitor applications, Applied Physics Letters 106 (25) (2015) 252901. https://doi.org/10.1063/1.4922947.
[73] Z. Shen, X. Wang, B. Luo, L. Li, $BaTiO_3$–$BiYbO_3$ perovskite materials for energy storage applications, J. Mater. Chem. A 3 (35) (2015) 18146–18153, https://doi.org/10.1039/C5TA03614C.
[74] T. Wang, L. Jin, C. Li, Q. Hu, X. Wei, D. Lupascu, Relaxor ferroelectric BaTiO3–Bi(Mg2/3Nb1/3)O3 ceramics for energy storage application, J. Am. Ceram. Soc. 98 (2) (2015) 559–566, https://doi.org/10.1111/jace.13325.
[75] Q.i. Xu, H. Liu, Z. Song, X. Huang, A. Ullah, L. Zhang, J. Xie, H. Hao, M. Cao, Z. Yao, A new energy-storage ceramic system based on $Bi_{0.5}Na_{0.5}TiO_3$ ternary solid solution, J Mater Sci: Mater Electron 27 (1) (2016) 322–329.
[76] D. Zheng, R. Zuo, D. Zhang, Y. Li, X. Tan, Novel BiFeO3-BaTiO3-Ba(Mg1/3Nb2/3)O3 Lead-Free Relaxor Ferroelectric Ceramics for Energy-Storage Capacitors, J. Am. Ceram. Soc. 98 (9) (2015) 2692–2695, https://doi.org/10.1111/jace.13737.

[77] X. Zhou, C. Yuan, Q. Li, Q. Feng, C. Zhou, X. Liu, Y. Yang, G. Chen, Energy storage properties and electrical behavior of lead-free (1−x) $Ba_{0.04}Bi_{0.48}Na_{0.48}TiO_3$–x$SrZrO_3$ ceramics, Journal of Materials Science: Materials in Electronics 27(4) (2015) 3948-3956. https://doi.org/10.1007/s10854-015-4247-x.

[78] P. Chen, B. Chu, Improvement of dielectric and energy storage properties in Bi(Mg 1/2 Ti 1/2)O 3 -modified (Na 1/2 Bi 1/2) 0.92 Ba 0.08 TiO 3 ceramics, J. Eur. Ceram. Soc. 36 (1) (2016) 81–88.

[79] B. Qu, H. Du, Z. Yang, Lead-free relaxor ferroelectric ceramics with high optical transparency and energy storage ability, J. Mater. Chem. C 4 (9) (2016) 1795–1803, https://doi.org/10.1039/C5TC04005A.

[80] B. Qu, H. Du, Z. Yang, Q. Liu, T. Liu, Enhanced dielectric breakdown strength and energy storage density in lead-free relaxor ferroelectric ceramics prepared using transition liquid phase sintering, RSC Adv. 6 (41) (2016) 34381–34389, https://doi.org/10.1039/C6RA01919F.

[81] L. Wu, X. Wang, L. Li, Lead-free BaTiO3–Bi(Zn2/3Nb1/3)O3 weakly coupled relaxor ferroelectric materials for energy storage, RSC Adv. 6 (17) (2016) 14273–14282, https://doi.org/10.1039/C5RA21261H.

[82] Q. Xu, H. Liu, L. Zhang, J. Xie, H. Hao, M. Cao, Z. Yao, M.T. Lanagan, Structure and electrical properties of lead-free $Bi_{0.5}Na_{0.5}TiO_3$-based ceramics for energy-storage applications, RSC Advances 6(64) (2016) 59280-59291. https://doi.org/10.1039/C6RA11744A.

[83] Z. Yang, H. Du, S. Qu, Y. Hou, H. Ma, J. Wang, J. Wang, X. Wei, Z. Xu, Significantly enhanced recoverable energy storage density in potassium–sodium niobate-based lead free ceramics, J. Mater. Chem. A 4 (36) (2016) 13778–13785, https://doi.org/10.1039/C6TA04107H.

[84] T. Shao, H. Du, H. Ma, S. Qu, J. Wang, J. Wang, X. Wei, Z. Xu, Potassium–sodium niobate based lead-free ceramics: novel electrical energy storage materials, J. Mater. Chem. A 5 (2) (2017) 554–563, https://doi.org/10.1039/C6TA07803F.

[85] H. Yang, F. Yan, Y. Lin, T. Wang, F. Wang, High energy storage density over a broad temperature range in sodium bismuth titanate-based lead-free ceramics, Sci Rep 7 (1) (2017) 8726, https://doi.org/10.1038/s41598-017-06966-7.

[86] D. Zheng, R. Zuo, Enhanced energy storage properties in La(Mg1/2Ti1/2)O3-modified BiFeO3-BaTiO3 lead-free relaxor ferroelectric ceramics within a wide temperature range, J. Eur. Ceram. Soc. 37 (1) (2017) 413–418, https://doi.org/10.1016/j.jeurceramsoc.2016.08.021.

[87] M. Zhou, R. Liang, Z. Zhou, X. Dong, Novel $BaTiO_3$-based lead-free ceramic capacitors featuring high energy storage density, high power density, and excellent stability, J. Mater. Chem. C 6 (31) (2018) 8528–8537, https://doi.org/10.1039/C8TC03003K.

[88] L. Chen, F. Long, H. Qi, H. Liu, S. Deng, J. Chen, Outstanding Energy Storage Performance in High-Hardness (Bi0.5K0.5)TiO3 -Based Lead-Free Relaxors via Multi-Scale Synergistic Design, Adv. Funct. Mater. 32 (9) (2022) 2110478, https://doi.org/10.1002/adfm.202110478.

[89] Z. He, S. Shi, Z. Pan, L. Tang, J. Zhao, Y. Shen, D.i. Hu, Y. Chen, P. Li, J. Liu, J. Zhai, Low electric field induced high energy storage capability of the free-lead relaxor ferroelectric $0.94Bi_{0.5}Na_{0.5}TiO_3$-$0.06BaTiO_3$-based ceramics, Ceram. Int. 47 (8) (2021) 11611–11617.

[90] S. Li, T. Hu, H. Nie, Z. Fu, C. Xu, F. Xu, G. Wang, X. Dong, Giant energy density and high efficiency achieved in silver niobate-based lead-free antiferroelectric ceramic capacitors via domain engineering, Energy Storage Mater. 34 (2021) 417–426, https://doi.org/10.1016/j.ensm.2020.09.021.

[91] L. Chen, S. Deng, H. Liu, J. Wu, H. Qi, J. Chen, Giant energy-storage density with ultrahigh efficiency in lead-free relaxors via high-entropy design, Nat. Commun. 13 (1) (2022) 3089, https://doi.org/10.1038/s41467-022-30821-7.